

## MEAN TEMPERATURE PROFILE AT THE ENTRANCE OF A THERMOACOUSTIC STACKED SCREEN HEAT EXCHANGER

*S. Bühler*<sup>1</sup>, *D. Wilcox*<sup>2</sup>, *J.P. Oosterhuis*<sup>1</sup>, *T.H. van der Meer*<sup>1</sup>

<sup>1</sup> *Thermal Engineering, University of Twente,  
P.O. Box 217 – 7500AE Enschede, The Netherlands*

<sup>2</sup> *Chart Inc.-Qdrive, Troy, New York 12180, USA*

In thermoacoustic devices, the thermoacoustic effect occurs in the regenerator placed between two heat exchangers. The entrance effects of such heat exchanger are investigated with two computational fluid dynamics (CFD) test cases. The first CFD test case models an ideal heat exchanger adjacent to an open space. The influence of heat conduction on the mean temperature is shown. The second test case models two screens of a stacked screen heat exchanger as two inline cylinders. Three different openings are investigated. The mean temperature profile is compared to the numerical solution of a reduced model equation. It is shown that viscous effects do not influence the mean temperature profile at low amplitude.

**Introduction.** Thermoacoustic engines are of raising interest in recent years as they promise to be a reliable alternative to traditional Stirling engines. Thermoacoustic engines can achieve this high reliability as the number of moving parts is reduced compared to their counter parts. This is possible as the displacement and compression are not executed by displacer and power pistons, but by an acoustic wave thermally interacting with a solid (i.e. a regenerator). Furthermore, thermoacoustic engines using liquid metals as a working fluid even promise to produce electric power without any moving part, as the moving liquid metal can be used in a magnetohydrodynamic transducer to create electric power [2]. In thermoacoustic devices, liquid metals like sodium have additional advantages as they have extremely low Prandtl numbers, high densities and moderate expansion coefficients [1].

Thermoacoustic engines convert heat into acoustic power. The thermoacoustic effect occurs in the regenerator, which is situated between two heat exchangers. On the other side of the hot heat exchanger a thermal buffer tube is placed to insulate the hot heat exchanger from the secondary ambient heat exchanger, while transferring the acoustic power [3]. Storch *et al.* [4] reported a distorted temperature profile within the thermal buffer tube, which does not follow the linear thermoacoustic theory derived by Rott [5] and reviewed by Swift [6]. This is due to the violation of the assumption that the displacement amplitude  $\xi_1$  is much smaller than all other relevant dimensions in the wave propagation direction. In common thermoacoustic engines, the length of the heat exchanger is comparable with the displacement amplitude  $\xi_1$  [6]. In this case, the convective effects  $(u\nabla)T$  at the entrance of the heat exchangers are not negligible as they lead to a change in mean temperature, which can be of the order of the adiabatic temperature oscillation. This nonlinear effect leads to an increase in thermal losses, through the thermal buffer tube [4].

The change in mean temperature is qualitatively explained by Swift [6] and Kittel *et al.* [7] by following gas parcels in Lagrangian coordinates which start within two displacements amplitudes of the entrance of a heat exchanger. Summing the temperature of the gas parcels at one position in Eulerian coordinates, the mean temperature profile close to the entrance of the heat exchanger can be ob-

tained. This leads to a joining condition in the mean temperature, which is widely accepted and implemented in one-dimensional codes like DeltaEC [8]. Analytical solutions are derived by Matveev *et al.* [9] and Gusev *et al.* [10] for a simplified case, in which both the heat conduction in the wave propagation direction and the viscous effects are neglected. Next to the analytical solution, numerical models that also include heat conduction in the wave propagation direction are presented by Matveev *et al.* [11] and Berson *et al.* [12]. These results are compared to experimental results and showed good agreement for travelling wave phasing.

In this paper, the interaction of the working fluid with a heat exchanger is investigated with computational fluid dynamics (CFD) simulations. It is shown that CFD can be used to predict the changes in mean temperature close to the heat exchanger. The simulations are extended from an ideal heat exchanger to a reduced model of a stacked screen heat exchanger. Two CFD models are presented: the first models an ideal heat exchanger with an open space. The influence of heat conduction is shown with this test case and the dedicated boundary condition is validated. The second CFD model presented in this paper models a stacked screen heat exchanger. This model includes the changes of the cross-sectional area and the viscous effects. The results of the models are compared to the analytical solution of Matveev *et al.* [9] and to a numerical model similar to the one presented in [11] and [12].

**1. Method.** Two CFD models and two simplified models are applied to estimate the mean temperature profile close to the heat exchanger in a thermoacoustic engine. The CFD models are based on the commercial finite volume code ANSYS Fluent 14.0 [13]. In both models, the working fluid is helium at a mean pressure of  $p_0 = 1$  atm and at a temperature of  $T_0 = 300$  K. In total, five acoustic periods are simulated and the mean temperature is calculated by averaging the last period. A travelling wave with a frequency of  $f = 100$  Hz is modeled. The wave enters at the left side of the domain with a pressure amplitude of  $p_1 = 250$  Pa and leaves it at the right through a non-reflecting boundary.

*1.1. CFD models.* The first test case consists of an ideal heat exchanger, with an open area. The CFD model and its boundary conditions are presented in Fig. 1. The ideal heat exchanger at the left and the non-reflecting boundary condition at the right of the domain are modelled with help of a dedicated acoustic boundary condition implemented via a User Defined Function (UDF) in ANSYS Fluent 14.0, which is similar to the one described by Liao [14]. The underlying idea is that the forward and the backward travelling wave is calculated at a point inside the domain, such that the wave leaving the domain at the boundary one time step later is known. In the present model, the left boundary condition imposes the pressure at the boundary such that a travelling wave is introduced with a pressure amplitude of  $p_1 = 250$  Pa. The introduced wave travels through the computational domain and exits at the right through another non-reflecting boundary condition. The two acoustic boundary conditions at the extremities of the domain differ in the way the temperature of the incoming fluid is calculated. At the left boundary,

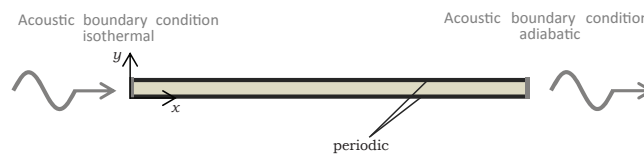


*Fig. 1.* Boundary conditions of the ideal heat exchanger model.

it is assumed that the incoming fluid is isothermal, in order to model the ideal heat exchanger. At the right boundary, the temperature of the incoming fluid is calculated from the pressure, assuming adiabatic wave propagation. The horizontal boundary conditions are set to be periodic. The characteristic length in the wave propagation direction is the displacement amplitude  $\xi_1$ , which is estimated in this paper assuming a purely travelling wave as [6]:

$$\xi_1 = \frac{u_1}{\omega} = \frac{p_1}{\rho_0 c_0 2\pi f} = 2.4 \text{ mm.} \quad (1)$$

The total domain is five displacement amplitudes  $\xi_1$  long and  $0.04\xi_1$  high. The domain is discretized using 100 elements per displacement amplitude in both spatial directions, so 500 by 4 elements, yielding to a total mesh size of 2000 elements. The time step size is set to  $\Delta t = 2.0 \times 10^{-6}$  s, which corresponds to 5000 time steps per period. The domain is initialized with zero velocity and a mean temperature of  $T_0 = 300$  K.

While the first model allows the investigation of an ideal heat exchanger, the second models a more realistic heat exchanger: a stacked screen heat exchanger. In this case, the thermal contact is not ideal and viscous losses occur. As the main focus is on the entrance effects, the heat exchanger is modelled in a simplified form and only two screens are taken into account. Neglecting gravity effects and the effects of the duct, where the heat exchanger is housed, and by implementing periodic boundary conditions, the mesh can be reduced to one square repetitive unit. In a first approach, this cell is further reduced to a two dimensional array of cylinders, representing the individual wires of the screen. The simplified model is shown in Fig. 2. As was the case in the previous model, the boundary conditions are chosen such that an acoustic wave with a pressure amplitude of  $p_1 = 250$  Pa enters the domain at the left and exits at the right without reflection. Unlike in the first model, no ideal heat exchanger boundary condition is applied. The temperature of the incoming fluid is calculated from the pressure at the boundary assuming adiabatic wave propagation on both sides. The cylinders modelling the stacked screens are assumed isothermal and a no-slip velocity boundary is imposed. The radius is determined from available mesh screens with an opening of two thermal penetration depth  $\delta_\kappa$ . As the heat capacity of the metal wire is high compared to the working gas, the wire radius is not defined from a thermal point of view, but rather a production point of view. In this paper, the radius  $R = 0.046\xi_1$  is chosen from an available meshed screen. Assuming that the screens are perfectly aligned and reasonably packed, the maximum distance between two wires is  $4R$ . For this reason, the centers of the cylinders are separated by  $6R$  in the model. The domain length has to be chosen such that the boundaries of the computational domain are at least two displacement amplitudes  $\xi_1$  away from the cylinders. In the present model, the total length is  $L = 7.5\xi_1$ . Three different screen openings are investigated in this paper in order to show the influence of the thermal contact on the entrance effects. The different domain heights are

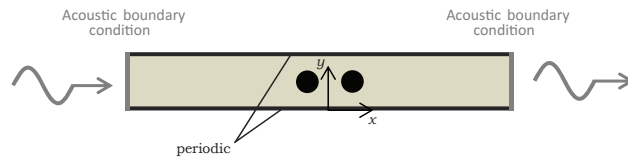


Fig. 2. Boundary conditions of the stacked screen heat exchanger model.

chosen such that the half spacing is approximately one third, one and two thermal penetration depths. The corresponding domain heights are:  $H_1 = 6R$ ,  $H_2 = 16R$  and  $H_3 = 32R$ , respectively.

The domains are discretized with quadrilateral O-grids around the two cylinders and rectangular grids further away from the cylinders. The rectangular grids at the left and right of the cylinders are discretized with rectangular elements that grow with a geometric factor of 1.1 towards the boundaries and have a constant height of  $\Delta y/\xi_1 = 5.7 \times 10^{-3}$ . The maximum element size in the axial direction is  $\Delta x/\xi_1 = 0.3$  at the boundary. The meshes around the cylinders are quadrilateral and have a growing factor of 1.2 in the radial direction. The smallest element size is  $\Delta r/\xi_1 = 2.2 \times 10^{-4}$ . There are 96 elements over the perimeter of the cylinder. The meshes have a total of 12553, 23673 and 41465 nodes, respectively. The time step size is set to  $\Delta t = 1.5 \times 10^{-6}$  s, which corresponds to more than 6600 time steps per period.

*1.2. Simplified models.* The aforementioned CFD models are compared against two simplified models. The first is the analytical solution derived by Matveev *et al.* [9]. The main assumptions for the derivation are

- No viscous wall effects occur, one dimensional acoustics.
- No heat conduction besides the temperature gradient imposed by the heat exchangers.
- The pressure is spatially constant.

In the CFD models presented above, the travelling wave is investigated with no temperature gradient. In this case, the analytical solution for the mean temperature can be written as [9]:

$$T_m(x) = T_0 - \frac{2}{\pi} \left( 1 - \left( \frac{x}{2\xi_1} \right)^{\pi/2} \right) \frac{\gamma - 1}{\gamma} \frac{p_1}{p_0} T_0. \quad (2)$$

In this paper, the Eulerian coordinates are chosen, similar to Berson *et al.* [12]. The following temperature equation is solved

$$\frac{\partial T}{\partial t} = \frac{\gamma - 1}{\gamma} \frac{T}{p} \frac{\partial p}{\partial t} - u \frac{\partial T}{\partial x} + \frac{\gamma - 1}{\gamma} k \frac{T}{p} \left( \frac{\partial^2 T}{\partial x^2} \right) + K (T_{\text{HX}} - T), \quad (3)$$

where the factor  $K$  is the heat transfer coefficient between the heat exchanger and the fluid. Outside the heat exchanger,  $K$  is set to zero. The pressure and the velocity are imposed assuming a travelling wave with no spatial variations,

$$p(t) = p_0 + p_1 \sin(\omega t), \quad (4)$$

$$u(t) = u_1 \sin(\omega t). \quad (5)$$

The temperature equation is solved with the MATLAB function *pdepe()*, which solves initial-boundary problems for parabolic partial differential equations in one-dimension. The temperature is calculated for five periods and the temperature is averaged over the last period to obtain the mean temperature profile.

**2. Results and discussion.** The results for the two CFD models are discussed separately in the following subsections. Furthermore, the CFD models are compared to the one-dimensional models.

*2.1. Ideal heat exchanger model.* In this section, the simulation results of the ideal heat exchanger model are presented. The changes in mean temperature normalized by the adiabatic temperature amplitude are shown in Fig. 3 over the dimensionless axial coordinate  $x/\xi_1$ . The mean temperature is calculated from

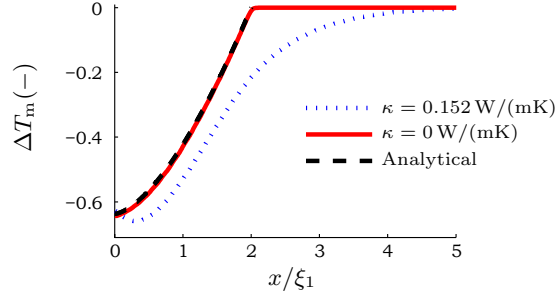


*Fig. 3.* Changes in mean temperature normalized by the adiabatic temperature amplitude and plotted over the dimensionless axial coordinate  $x/\xi_1$  in the case of the ideal heat exchanger model.

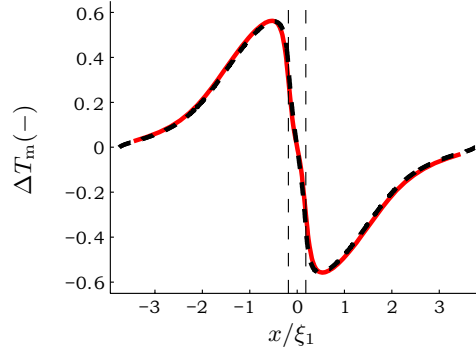


*Fig. 4.* Changes in mean temperature normalized by the adiabatic temperature amplitude and plotted over the dimensionless axial coordinate  $x/\xi_1$  in the case of the stacked screen model. The mean of the temperature is taken over the fifth period. Results from model (dashed black line) and CFD simulation with a domain height of  $H = 6R$  (red full line). Vertical dashed lines indicate the extremities of the stacked screens.

the data of the fifth period. The red line shows the results from CFD with zero heat conductivity; in this case, the effect of the ideal heat exchanger only extends within two displacement amplitudes  $\xi_1$ . The black dashed line in Fig. 3 shows the analytical solution given in Eq. (2). The analytical solution overlays the red line, as in both cases no heat conduction is assumed. It can be concluded that the applied boundary condition is correctly implemented and that the boundary can model an ideal heat exchanger. This boundary can thus also be used in the future work to model individual components of the thermoacoustic engine, such as the thermal buffer tube. The blue dotted line shows the mean temperature using a heat conductivity of  $\kappa = 0.152 \text{ W}/(\text{mK})$  which corresponds to helium. A clear minimum in the mean temperature can be seen within one displacement amplitude of the ideal heat exchanger. Furthermore, at the right of the domain heat is conducted towards the outside of the domain. It can be concluded that heat conduction shifts the minimum temperature away from the heat exchanger. Heat is conducted into the rest of the domain and the mean temperature profile is influenced beyond two displacements amplitudes  $\xi_1$ . This indicates that additional losses are introduced due to the conduction over the right boundary, similar to what was reported experimentally by Storch *et al.* [4].

**2.2. Stacked screen model.** In this section, the results for the stacked screen CFD model are discussed. First, the simulation is validated with the simplified model. The results are shown in Fig. 4, where the changes in mean temperature

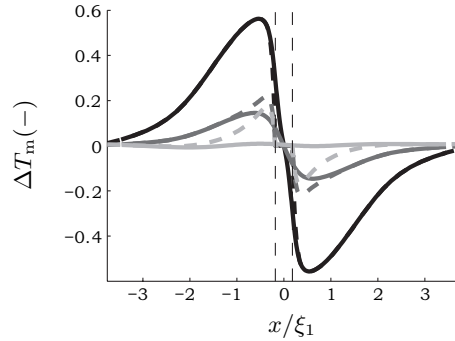


*Fig. 5.* Changes in mean temperature normalized by the adiabatic temperature amplitude and plotted over the dimensionless axial coordinate  $x/\xi_1$  in the case of the stacked screen model. The mean of the temperature is taken over the fifth period. The black lines, the dark gray lines and the light gray lines show the results for the domain heights  $H = 6R$ ,  $H = 16R$  and  $H = 32R$ , respectively. The dashed lines show the mean temperature at  $y = H/2$  and the solid lines show the mean temperature at the height  $y = 0$ . Vertical dashed lines indicate the extremities of the stacked screens.

normalized by the adiabatic temperature amplitude are plotted over the axial coordinate  $x/\xi_1$ . The mean temperature is calculated from the data of the fifth period. The solid red line shows the results of the CFD simulation with the smallest screen opening ( $H = 6R$ ), while the black dashed line shows the numerical solution of the simplified model. The heat transfer coefficient in the simplified model  $K$  is chosen such that it fits the CFD simulation. The two mean temperature profiles are in good agreement with each other. It can be concluded that the CFD model is correctly implemented. Moreover, the temperature averaged over one period at earlier periods (not shown here) shows good agreement. In other words, the viscous effects, which are neglected in the simplified model, do not have a large influence on the mean temperature profile at low pressure amplitudes.

In the next step, the simulations with different screen openings are compared with each other. Due to the different screen openings, the thermal contact between the heat exchanger and the fluid changes and leads to different mean temperature profiles. Fig. 5 shows the changes in mean temperature over the dimensionless axial coordinate  $x/\xi_1$ . The mean of the temperature is taken over the fifth period. The dashed lines show the mean temperature at the height  $y = H/2$  and the solid lines show the mean temperature at the height  $y = 0$ . The different colors indicate the different openings of the screens. The center between the two cylinders modelling the stacked screen heat exchanger is located at  $(x/\xi_1) = 0$  and the extremities of them are indicated by the vertical dashed lines. All profiles are point symmetric around the origin and the entrance effects on both sides of the heat exchanger are modelled. It can be seen that the temperature overshoot is smallest in the case of the largest screen opening ( $H = 32R$ ), which corresponds to the weakest thermal contact. The smaller is the screen opening, the higher becomes the temperature overshoot. The reason for this is shown in Fig. 6, where the thermodynamic cycles are given for gas parcels starting at the location  $x = 0$ ,  $y = 0$ . The cycle that the gas parcels undergo is similar to the one of an ideal Brayton cycle [15]. For weaker thermal contact, less heat is transferred during the isobaric stages. The surface enclosed in the  $p$ - $v$ -diagram is smaller. As less heat is pumped, the temperature overshoot is smaller. In the case of the largest screen opening, the mean temperature profile at  $y = 0$  (solid light gray line in Fig. 5) is nearly constant as the fluid at this height is outside of the thermal boundary layer and does not

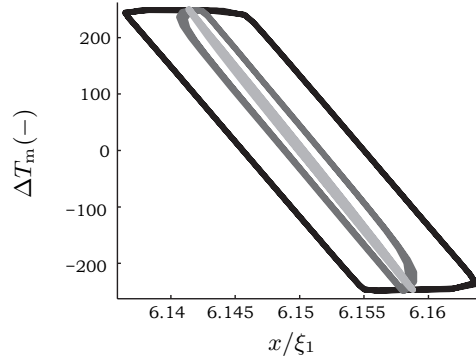


Fig. 6.  $p - v$ -diagram for the fluid parcels starting at  $x = 0$ ,  $y = 0$  in the stacked screen model. The black lines, the dark gray line and the light gray show the results for the domain heights  $H = 6R$ ,  $H = 16R$  and  $H = 32R$ , respectively.

interact with the cylinders. In the case of the smallest opening, the whole fluid has close thermal contact with the heat exchanger. As the whole fluid takes part in the pumping, the mean temperature at the two different heights is nearly the same.

The maximum overshoot from the simulation can also be compared with the results from the ideal heat exchanger model illustrated in Fig. 1. The overshoot in the ideal case is higher than in the cases with non-ideal thermal contact. In the case of the smallest screen opening, which corresponds to half-spacing between the cylinder of  $(1/3) \delta_\kappa$ , the temperature overshoot reaches more than 80% of the value of an ideal heat exchanger.

**3. Conclusion.** A first step is taken with CFD to investigate the entrance effects near a stacked screen heat exchanger. Two CFD models are presented. From the first model it can be concluded that the dedicated boundary condition, modelling the ideal heat exchanger, was correctly implemented and worked well. In the future work, this boundary condition can be used to simulate the flow field in individual components of a thermoacoustic engine like the thermal buffer tube. Furthermore, with the first model it is shown that heat conduction flattens the mean temperature profile compared to the case without heat conduction and leads to a different position of the maximum temperature overshoot. From the second model it can be shown that solving only the one dimensional heat equation (Eq. (3)) for a given pressure and velocity gives similar results compared to CFD. Hence, viscous effects do not play an important role at low amplitudes. Furthermore, the influence of the opening of the meshed screens was investigated. The temperature overshoot is highest in the case of a close thermal contact, which corresponds to the smallest screen opening. In this case, the differences in mean temperatures over the height are the smallest, as the whole flow field takes part in the heat pumping.

In the future work, the regenerator model shall be extended such that high pressure amplitude simulations can be carried out including also various phasing between the pressure and the velocity. This will allow the investigation of the influence of vortex generation on the heat transfer in oscillating flows and provide a better understanding of the heat transfer in a stacked screen heat exchanger.

**Acknowledgements.** The authors would like to thank Agentschap NL for the financial support as part of the EOS-KTO program, project No. KTOT03009.

## References

- [1] G.W. SWIFT. A liquid-metal magnetohydrodynamic acoustic transducer. *The Journal of the Acoustical Society of America*, vol. 83 (1988), no. 1, pp. 350–361.
- [2] G.W. SWIFT. Thermoacoustic engines. *The Journal of the Acoustical Society of America*, vol. 84 (1988), no. 4, pp. 1145–1180.
- [3] S. BACKHAUS AND G.W. SWIFT. A thermoacoustic stirling heat engine. *Nature*, vol. 399 (1999), no. 6734, pp. 335–338.
- [4] P.J. STORCH, R. RADEBAUGH AND J.E. ZIMMERMAN. Analytical Model for Refrigeration Power of the Orifice Pulse Tube Refrigerator. *National Institute of Standards and Technology*. (US, 1990.)
- [5] N. ROTT. Thermoacoustics. *Advances in Applied Mechanics*, vol. 20 (1980), pp. 135–175.
- [6] G.W. SWIFT. Thermoacoustics: a unifying perspective for some engines and refrigerators. *Acoustical Society of America through the American Institute of Physics*, 2002.
- [7] P. KITTEL. The temperature profile within pulse tubes. *Advances in Cryogenic Engineering*, vol. 43 (1998), pp. 1927–1932.
- [8] B. WARD, J. CLARK, AND G. SWIFT. *Design Environment for Low-Amplitude Thermoacoustic Energy Conversion (DeltaEC) User Guide, Version 6.2* (Los Alamos National Laboratory, 2008).
- [9] K.I. MATVEEV, G.W. SWIFT, AND S. BACKHAUS. Analytical solution for temperature profiles at the ends of thermal buffer tubes. *Int. J. Heat and Mass Transfer*, vol. 50 (2007), pp. 897–901.
- [10] V. GUSEV *et al.* Thermal wave harmonics generation in the hydrodynamical heat transport in thermoacoustics. *The Journal of the Acoustical Society of America*, vol. 109 (2001), no. 1, pp. 84–90.
- [11] K.I. MATVEEV, G.W. SWIFT, AND S. BACKHAUS. Temperature near the interface between an ideal heat exchanger and a thermal buffer tube or pulse tube. *Int. J. Heat and Mass Transfer*, vol. 49 (2006), pp. 868–878.
- [12] A. BERSON, G. POIGNAND, AND S. BACKHAUS. Non-linear temperature field near the stack ends of a standing wave thermoacoustic refrigerator. *Int. J. Heat and Mass Transfer*, vol. 54 (2011), no. 2122, pp. 4730–4735.
- [13] ANSYS Inc., 275 Technology Drive Canonsburg, PA 15317. *ANSYS FLUENT 14.0 User's Guide, 2013*.
- [14] Z.-P. LIAO. Extrapolation non-reflecting boundary conditions. *Wave Motion*, vol. 24 (1996), no. 2, pp. 117–138.
- [15] C. WU. *Thermodynamics and Heat Power Cycles: A Cognitive Engineering Approach*. (Nova Science Publishers, Inc., 2007).

Received 31.10.2014